Rock Mech. Rock Engng. (2004) 37 (4), 251–275
DOI 10.1007/s00603-003-0022-z

Rock Mechanics and Rock Engineering
Printed in Austria

Influence of Heterogeneity of Mechanical Properties on Hydraulic Fracturing in Permeable Rocks

By

T. H. Yang[1], **L. G. Tham**[2], **C. A. Tang**[1], **Z. Z. Liang**[1], and **Y. Tsui**[2]

[1] Center for Rock Instability and Seismicity Research, Northeastern University, Shenyang, P.R. China
[2] Department of Civil Engineering, The University of Hong Kong, Hong Kong, P.R. China

Received March 15, 2003; accepted October 1, 2003
Published online January 9, 2004

Summary

Numerical simulations of circular holes under internal hydraulic pressure are carried out to investigate the hydraulic fracture initiation, propagation and breakdown behavior in rocks. The hydraulic pressure increases at a constant rate. The heterogeneity of the rocks is taken into account in the study by varying the homogeneity index. In addition, the permeability is varied with the states of stress and fracture. The simulations are conducted by using a finite element code, F-RFPA^{2D}, which couples the flow, stress and damage analyses. The simulation results suggest that the fracture initiation and propagation, the roughness of the fracture path and the breakdown pressure are influenced considerably by the heterogeneity of rocks. The hole diameter elongation and the stress field evolution around the fracture tip during the fracture propagation can also provide useful information for the interpretation of the hydraulic fracturing behaviour.

Keywords: Hydraulic fracturing, heterogeneity, permeable rocks, Weibull's function.

List of Symbols

σ_1	major principal stress
σ_3	minor principal stress
σ_t	tensile strength of the rock
σ_c	compressive strength of the rock
s	strength parameter or elastic modulus of the element
s_0	mean strength parameter or elastic modulus of the element
m	homogeneity index
σ_{ij}	total stress in the ij-plane

X_j body force in the j-th direction
ε_{ij} strain in the ij-plane
u_i displacement in the i-th direction
σ'_{ij} effective stress in the ij-plane
p pore pressure
α coefficient of pore-fluid presssure
λ Lame coefficient
G shear modulus
δ_{ij} Kronecher constant
k coefficient of permeability
k_i initial coefficient of permeability
Q Biot's constant
β material constant
ξ material constant
E_0 elastic modulus of the undamaged element
E elastic modulus of the damaged element
ν Poisson's ratio
ϕ friction angle
σ_{cr} total stress in the ij-plane
σ_{tr} residual tensile strength
σ_{cu} crack closure stress
Δd_{pa} the diameter elongation of parallel to the crack orientation
Δd_{pe} the diameter elongation of perpendicular to the crack orientation
L_U the unstable crack length
P_i fracture initiation pressure
P_b breakdown pressure
P_u unstable fracture propagation pressure

1. Introduction

Hydraulic fracturing has been widely used to determine in-situ stresses in rock masses and stimulate reservoir production. Understanding hydraulic fracture mechanisms and, then, finding ways to predict the geometry of the hydraulically induced fracture and the initiation pressure are important both for stress measurements and for improving well production. Different theories for hydraulic fracturing were proposed, and the oldest one and the most frequently used one is that proposed by Hubbert and Willis (1957). Although Haimson (1968) improved this theory by taking into account the effect of fluid penetration, the improvements (Zoback and Pollard, 1978) were not sufficient for explaining the hydraulic fracturing results published by Haimson and Fairhurst (1969) and others (Degue and Ladanyi, 2000). Among many of the other theories, the one based on Linear Elastic Fracture Mechanics (LEFM) was also used (Lockner and Byerlee, 1977; Aamodt and Potter, 1978; Zoback and Pollard, 1978; Rummel, 1987; Rummel and Hansen, 1989; Rummel et al., 1995). This theory considers a pressurized hole in an infinite space and the existence of only two symmetric radial cracks. Based on this LEFM approach, Degue and Ladanyi (2000) proposed a new theory by taking into account the effect of fluid penetration and the pressurization rate.

There are at least two drawbacks in most of the hydraulic fracture theories. First, the materials studied in most of the hydraulic fracture models are assumed to be impermeable. Therefore, the theories cannot explain the effect of fluid permeability on the hydraulic fracture behavior. Generally speaking, in the case of an impermeable

rock, the influence of permeability on fracture behavior may be ignored. The pressure – time curve is quite sufficient for determining the breakdown pressure (Charlez, 1991). Fracture initiation is characterized by a sharp peak which is then followed by a pressure drop. This peak is obviously related to unstable fracture propagation. However, Charlez (1991) pointed out that equilibrium between the well and the rock formation is continuously maintained in the permeable rocks as the fluid percolate through them. As a result, fracture initiation is sometimes stable. Therefore, it is necessary to take into account the flow behaviour in the analyses even for rocks with low permeability. For rock samples with low permeability, experimental results show that there is no drastic change in permeability as the loading stress increases within the elastic deformation range. However, significant permeability changes occur after the maximum strength of the rocks is reached (Zhang et al., 2000). Although there has been a great deal of interest in the last ten years in the coupling of fluid flow and geomechanical deformation processes in a single model where the interaction of flow and deformation (stress) can be modeled simultaneously, most hydraulic fracturing models remain uncoupled. However, in a large number of hydraulic fracturing problems there is a strong interaction between deformation (stress) and fluid flow. Standard modeling of these processes without considering the interaction effect can lead to significant errors in many cases (Zhang et al., 2000; Yale et al., 2000).

Secondly, the influence of heterogeneity existing in rock on the fracture pattern or hydraulic fracture path cannot be taken into account in most of the existing flow-coupled models. It is well known that rock is a heterogeneous geological material containing many natural weaknesses, such as pores, grain boundaries, and pre-existing cracks. When rock is subjected to hydraulic loading, these pre-existing defects can induce crack or fracture growth, which can in turn change the structure of the rock and alter the fluid flow properties of the rock (Wang and Kemeny, 1994). This heterogeneity related flow properties influences the hydraulic fracturing behaviour in many ways. For example, in the rock immediately around the borehole or the initiated fracture tips, micro-cracks or micro-fractures may initiate and grow. Consequently, a highly permeable damage zone or crack propagation zone is created around the fracture tip.

Due to the difficulty in obtaining a complete analytical solution for hydraulic fracturing problems, numerical simulation methods are widely used. Sophisticated hydraulic fracturing simulators, which can model the fracturing process numerically either in two or three dimensions (Morale and Abou-Sayed, 1989; Advani et al., 1990; Kim and Yao, 1994), have been developed to optimize the benefit of the hydraulic fracturing treatment. Again, in these models, the influence of the permeability of rock on the fracture propagation is assumed to be negligible.

In previous papers, a theoretical model named FSD, which couples the flow, stress and damage, has been proposed and implemented in a Rock Failure Process Analysis numerical code, F-RFPA (Tang, 1997; Tang et al., 2002; Yang et al., 2001). In this paper, an improved FSD model is introduced and applied to study hydraulic fracturing in permeable and heterogeneous rocks. Analyses have been performed to simulate the hydraulic fracturing in rocks with various degrees of heterogeneity. The effects of the confinement stress ratio and the non-uniform stress field on hydraulic fracture

propagation are also investigated. The results indicate that both the rock heterogeneity and the permeability affect fracture initiation and propagation significantly, and that the simplistic assumption that rock is homogeneous and impermeable may apply to limited, but not general cases in hydraulic fracturing.

2. Theory

Based on general observation, a model of coupling between flow, stress and damage has been proposed (Tang, 1997; Tang et al., 2002; Yang et al., 2001). The formulation of the model is based on the following assumptions:

- The rock mass is fully saturated.
- The flow of the fluid is governed by the Biot's consolidation theory (Biot, 1941).
- The rock is assumed to be brittle-elastic material with residual strength, and its loading and unloading behaviour are described by elastic damage mechanics.
- An element is considered to fail in the tension mode when its minimum principal stress exceeds the tensile strength of the element, and to fail in the compression-shear mode when the shear stress satisfies the strength criterion defined by the Mohr Coulomb failure envelope, that is
  Tensile failure:
  $$\sigma_3 > -\sigma_t. \tag{1a}$$
  Compressive-shear failure:
  $$\sigma_1 - \sigma_3 \frac{1+\sin\phi}{1-\sin\phi} < \sigma_c, \tag{1b}$$
  where σ_1 and σ_3 are the major and minor principal stresses, ϕ is the friction angle, σ_t is the tensile strength and σ_c is the compressive strength.
- The permeability varies as function of the stress states in elastic deformation, and increases dramatically when the element fails (Tang et al., 2002; Yang et al., 2001).
- The local heterogeneity in the properties of rock masses is defined by the Weibull's function, that is (Tang, 1997)
  $$\varphi(s,m) = \frac{m}{s_0}\left(\frac{s}{s_0}\right)^{m-1} \exp\left[-\left(\frac{s}{s_0}\right)^m\right], \tag{2}$$
  where s is the element strength or elastic modulus, and s_0 is the mean strength parameter or mean elastic modulus of elements. The parameter m is defined as the homogeneity index. Figure 1 shows the variations of φ with respect to m and it is obvious that a higher m value represents a more homogeneous material.

2.1 Basic Equations

Coupled seepage and stress processes in saturated geological media can be interpreted with Biot's theory of consolidation (Biot, 1941; Louis, 1974; Brown, et al., 1998). By extending Biot's theory of consolidation to include stress effects on permeability, the following governing equations can be obtained (Biot, 1941):

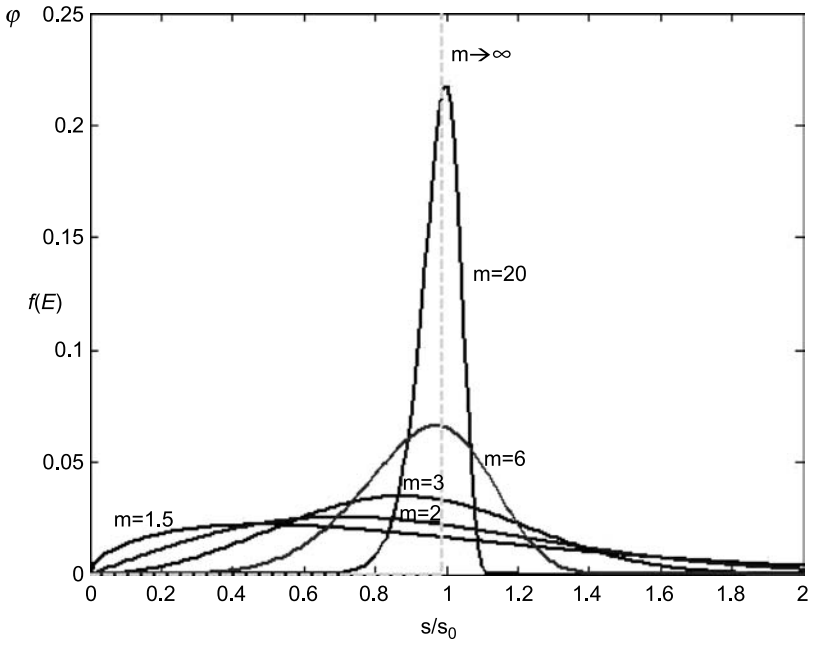

Fig. 1. Distribution of rock properties for different homogeneous indices

Balance equation:

$$\frac{\partial \sigma_{ij}}{\partial x_{ij}} + X_j = 0 \quad (i,j = 1,2,3) \tag{3}$$

where σ_{ij} is the stress and X_j is the body force in the j-th direction.
Geometrical equation:

$$\varepsilon_{ij} = \frac{1}{2}(u_{i,j} + u_{j,i}) \qquad \varepsilon_v = \varepsilon_{11} + \varepsilon_{22} + \varepsilon_{33}. \tag{4}$$

where ε_{ij} is the strain and u_i is the displacement in the i-th direction.
Constitutive equation:

$$\sigma'_{ij} = \sigma_{ij} - \alpha p \delta_{ij} = \lambda \delta_{ij} \varepsilon_v + 2G\varepsilon_{ij}, \tag{5}$$

where p is the pore pressure; α is the coefficient of pore-fluid pressure; λ is the Lame coefficient; G is the shear modulus and δ_{ij} is the Kronecher constant.
Seepage equation:

$$k\nabla^2 p = \frac{1}{Q}\frac{\partial p}{\partial t} - \alpha \frac{\partial \varepsilon_v}{\partial t}, \tag{6}$$

where k is the coefficient of permeability; Q is the Biot's constant.
Coupling equation:

$$k(\sigma, p) = \xi k_i e^{-\beta(\sigma_{ii}/3 - \alpha p)} \tag{7}$$

where k_i is the initial coefficient of permeability; β and ξ are material constants.

The above Eq. (3) to (6) are from the Biot's theory of consolidation (Biot, 1941). As experimental results show that the permeability is a function of stresses because the fracture aperture will change when the stress conditions vary, various permeability-stress relationships have been established (Zhang et al., 2000; Tang et al., 2002; Brown et al., 1998). In the present study, Eq. (7) is used to represent the influence of stress on permeability (Tang et al., 2002; Yang et al., 2001; Louis, 1974) by assuming that the permeability and stress follow a negative exponential function.

2.2 Implementation

In the study, the seepage and stress analyses were carried out by using the finite element method. The model was discretized into a large number of small square elements. The strength parameters and elastic modulus are randomly assigned to each element according to the Weibull's function (Eq. (2)). The model was loaded in a quasi-static fashion and a flow chart outlining the pertinent steps of the analysis is given in Fig. 2. At each loading increment, the seepage and stress equation in the elements were solved and the coupling analysis was performed. The stress field for each element was then examined. According to the stress level, the elements could be classified into four phases, as shown in Fig. 3:

(1) Elastic phase. If $\sigma_1 - \sigma_3 \frac{1+\sin\phi}{1-\sin\phi} < \sigma_c$ or $\sigma_3 > -\sigma_t$, the element is in the elastic phase and E_o and ν are the elastic modulus and Poisson's ratio of the element, respectively. As the permeability will decrease with the stress, it is assumed that $\alpha = 0$ and $\xi = 1$. Therefore, the permeability is given by

$$k(\sigma, p) = k_i e^{-\beta(\sigma_{ii}/3)}. \tag{7a}$$

Note that the k_i is assigned to the element in accordance to Eq. (2).

A comparison of the experimental results (Tang et al., 2002; Yang et al., 2001) shows that Eq. (7a) can approximately reflect the change in permeability fairly well (Fig. 4).

(2) Damage phase. If $\sigma_1 - \sigma_3 \frac{1+\sin\phi}{1-\sin\phi} \geq \sigma_c$, the element is in the damage phase and the failure is due to compression-shear. The elasticity modulus of the element will decrease according to the constitutive law for brittle failure (Fig. 3). Mathematically, the modulus can be written as

$$E = (1 - D)E_0, \tag{8}$$

where D represents the damage variable and E is the elastic modulus of the damaged elements. The damage variable can be defined as:

$$D = 1 - \frac{\sigma_{cr}}{E_0 \varepsilon} \tag{9}$$

where σ_{cr} is the residual compressive strength.

On the other hand, its permeability will undoubtedly increase as fractures begin to form and develop. To reflect the increase in permeability, ξ will be large. Denoting ξ by ξ_D, the permeability is calculated by

$$k(\sigma, p) = \xi_D k_i e^{-\beta(\sigma_{ii}/3)}. \tag{7b}$$

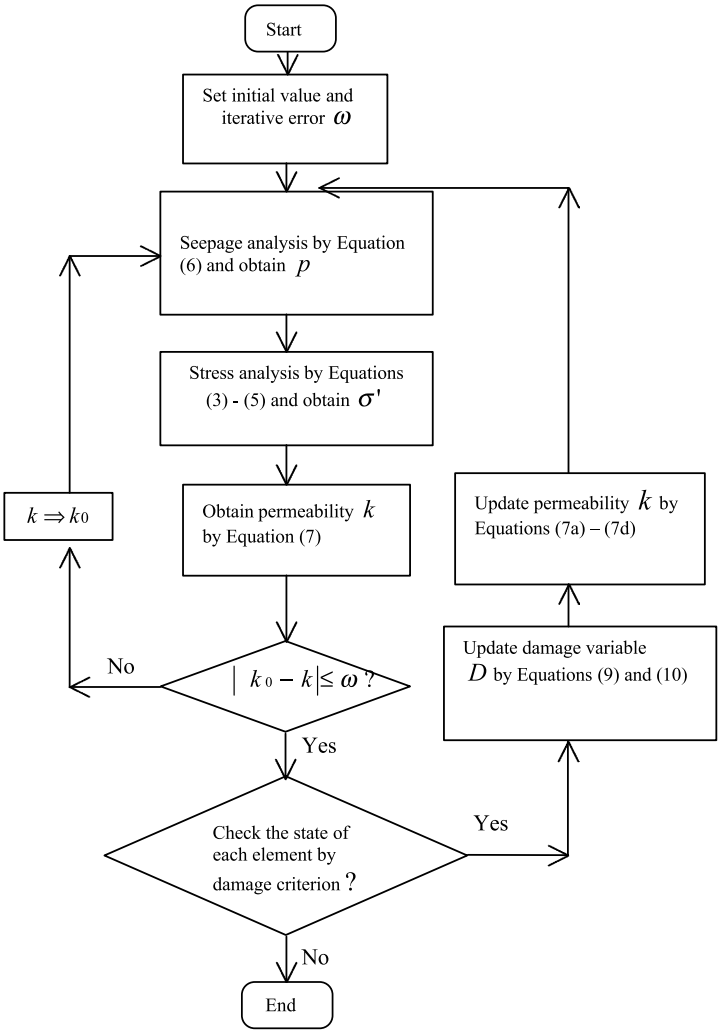

Fig. 2. The flow chart of the model

The variation in permeability predicted by Eq. (7b) with $\xi_D = 5$ for instance is in good agreement with the experimental results (Fig. 4).

If $\sigma_3 \le -\sigma_t$, the element fails in tensile failure mode. The elastic modulus can still be given by Eq. (8) but the damage variable has to be defined in terms of the residual tensile strength, σ_{tr}, that is

$$D = 1 - \frac{\sigma_{tr}}{E_0 \varepsilon}. \tag{10}$$

As the change in permeability should be independent on the mode of failure, it is assumed that the change in permeability after damage can also be given by Eq. (7b).

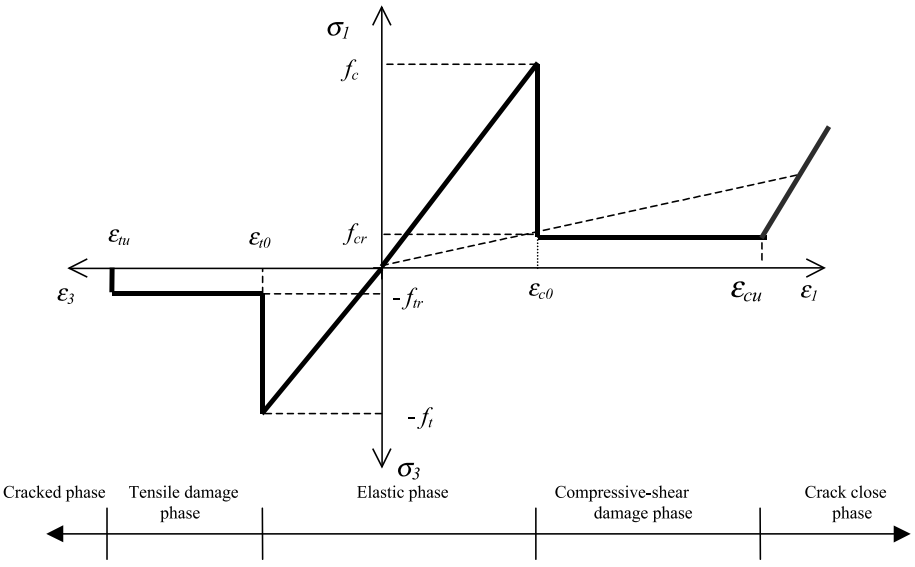

Fig. 3. Damage constitutive law

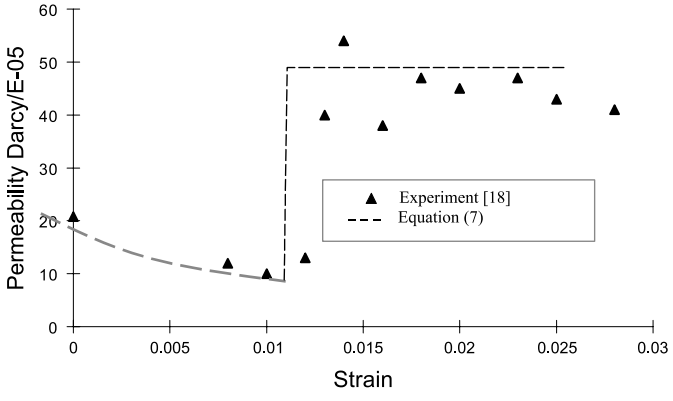

Fig. 4. Permeability-strain relation

(3) Cracked phase. In the cracked phase, macro fractures begin to form and the element will lose its capacity and stiffness. Therefore, the elastic modulus is assigned a very small value. Due to the existence of macro fractures (Zhu and Wong, 1999), the permeability will increase significantly and it can be obtained by $\xi = \xi_c$ and $\alpha = 1$, that is

$$k(\sigma, p) = \xi_c k_i e^{-\beta(\sigma_{ii}/3-p)} \tag{7c}$$

ξ_c is assumed to be very large.

(4) Crack closure phase. When the compressive strain of the crack element ε is greater than ε_{cu}, the crack can be considered to be closed. The element can transfer stress again and its modulus will increase as the compressive strain increases. The modulus can be calculated by

$$E = \frac{\sigma_{cr}}{\varepsilon_{cu}} \times \frac{\varepsilon}{\varepsilon_{cu}}. \tag{11}$$

To consider the permeability change in this phase (Zhu and Wong, 1999), we assume that ξ becomes small again and $\alpha = 0$, that is

$$k(\sigma, p) = \xi_{cc} k_i e^{-\beta(\sigma_{ii}/3)}, \tag{7d}$$

ξ_{cc} is assumed to be small.

As the elements may change from one phase to another, an iteration process is required to modify the elastic modulus and permeability by taking into account such changes. For a given hydraulic pressure, the stress and strain in individual element are solved at every loading step. At any step, if either shear or tension strength of an element is exceeded, the element can be considered to have failed irreversibly to initiate a new fracture or extend an old one. The element can then only carry the residual stress. For a failed element, its elastic modulus is considerably decreased and its permeability is considerably increased (Zhang et al., 2000). The stress and strain in individual elements are then solved again, which results in stress redistribution, until a new equilibrium is obtained. Thus, the evolution of this hydraulic system is determined, and the fracture initiation as well as propagation process are simulated.

Due to the high stress concentration at the crack tip or low strength elements, some weaker elements that are not on the fracture surface may fail to form micro-fractures that distribute in the vicinity of the fracture zone. Some of them may grow and join the main fracture, while others remain isolated beyond the main fracture. In most models such as the one developed by Kim and Yao (1994), the fluid pressure in the fracture is achieved by adding full pressure to the new main fracture surface instantaneously and no water pressure exists inside the isolated micro-fractures. In the present model, the fluid pressure in individual elements is calculated by solving coupling equation between stress and flow (Tang et al., 2002).

The number of failed elements and associated energy release (acoustic emission (AE) activities) accompanying hydraulic fracturing are also numerically recorded (Tang, 1997). Therefore, the fracture initiation can be pinpointed not only from the simulated breakdown pressure, but also from the sudden rise in the AE rate. In addition, one can trace the growth of the fractures from the locations of the acoustic emission activities.

2.3 Two Examples for Model Validation

A benchmark example of stress field and distribution in homogeneous and heterogeneous rock samples by applying fluid pressure in a hole has been analysed by using the present model. The geometry of the numerical samples is shown in Fig. 5. The horizontal stress, σ_x, and vertical stress, σ_y, are 1.0 MPa and 2.0 MPa, respectively. A fluid pressure, p_w, of 1.0 MPa is applied in the hole. The homogeneity index

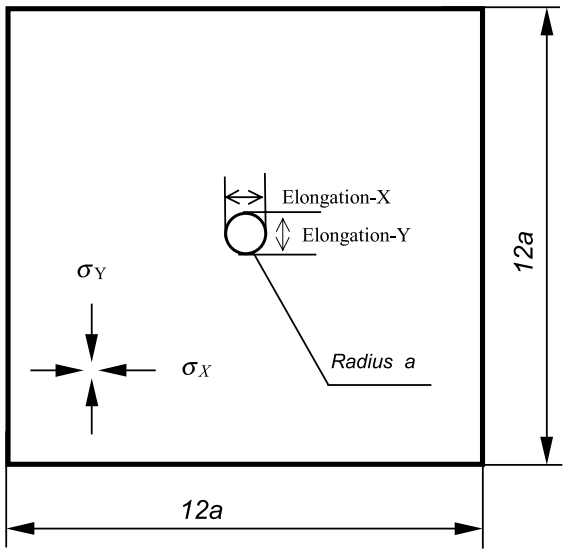

Fig. 5. Numerical model for hydraulic fracturing in rock sample ($\sigma_x = 1$ MPa, $\sigma_y = 2$ MPa, $p_w = 1$ MPa)

Table 1. Input parameters of rock properties in validation simulations

m	3, 1000
E_0 (*mean elastic modulus*)	6 GPa
v	0.25
ϕ_0 (*mean friction angle*)	30°
f_{co} (*mean compressive strength*)	60 MPa
f_{to} (*mean tensile strength*)	6 MPa
λ	0.1
k_0 (*mean coefficient of permeability*)	0.01 m/sec
α (*unfractured*)	0.0
α (*fractured*)	1.0
β	0.01

$m = 1000$ and $m = 3$ are chosen to simulate relatively homogeneous and relatively heterogeneous rocks, respectively. Other parameters adopted in the study are given in Table 1. The variations of the tangential and radial stress along the horizontal diameter are plotted in Fig. 6 for the homogeneous rock. The analytical solution [10] for the same problem of the homogeneous rock sample is also plotted in Fig. 6. From the figure, one can conclude that there is a very good agreement between the numerical and the analytical solutions. For a quantitative evaluation of the heterogeneity effect, we have shown in Fig. 7 the variation of the stresses along the horizontal diameter for both heterogeneous and homogeneous samples. Due to the variation in the elastic modulus of the elements, there are obvious fluctuations in the stresses though the average stresses are fairly close to the homogeneous one. The maximum fluctuation is over $\pm 50\%$.

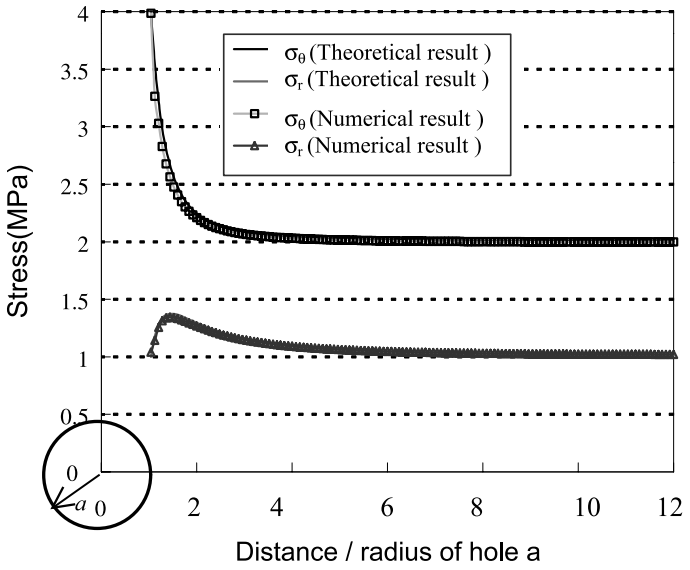

Fig. 6. Stress distribution along the horizontal diameter – numerical and analytical results ($\sigma_x = 1$ MPa, $\sigma_y = 2$ MPa, $p_w = 1$ MPa)

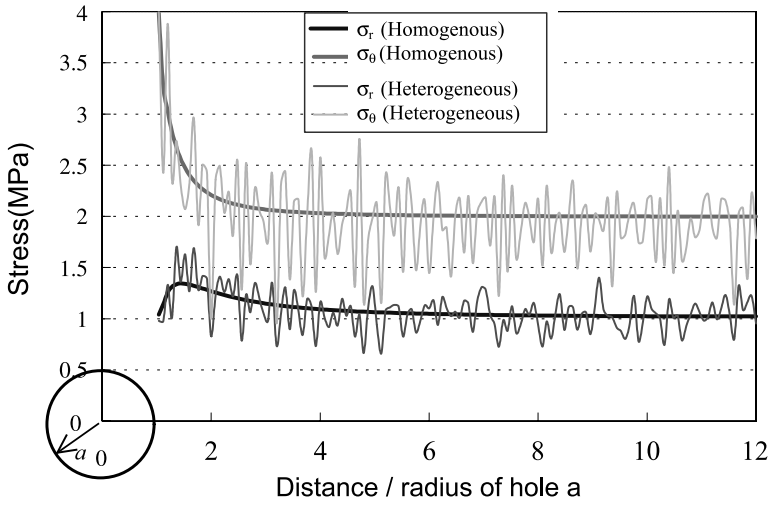

Fig. 7. Stress distribution along the horizontal diameter for heterogeneous and homogeneous rocks

Figure 8 shows the F-RFPA^{2D} code generated fringe patterns in both heterogeneous and homogeneous rock samples. The simulated figures clearly show that the heterogeneity of rock has strong influence on the stress fields. Since there is no

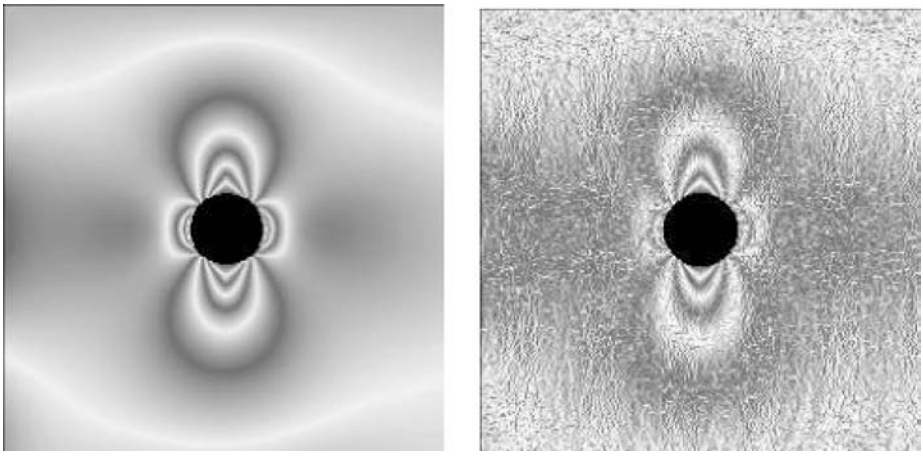

(a) homogeneous (b) heterogeneous sample

Fig. 8. Fingerprint of the major principal stress field in simulated homogeneous and heterogeneous rock samples ($\sigma_x = 1$ MPa, $\sigma_y = 2$ MPa, $p_w = 1$ MPa)

experimental method available for the fringe pattern in heterogeneous materials, the numerical obtained results are of great significance to improve our understanding of the stress field in a heterogeneous material.

The second example is to demonstrate the influence of fluid flow in the fractures on the breakdown pressure. The progressive growth of the fractures from a hole under

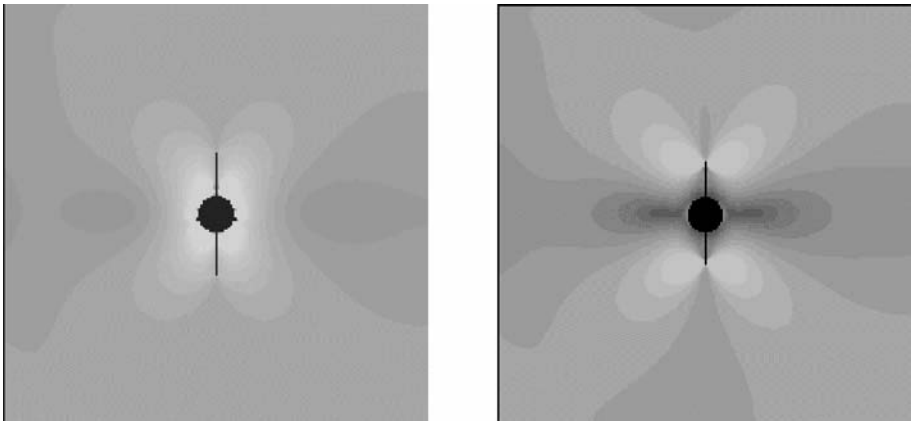

Case A
(Fluid is not allowed to flow into fracture)

Case B
(Fluid is allowed to flow into fracture)

Fig. 9. Propagation trajectory of the cracks in homogeneous samples ($\sigma_x = 1$ MPa, $\sigma_y = 2$ MPa)

the action of pressure with or without fluid flowing into the fractures is investigated. The parameters adopted in the analysis are also given in Table 1. Two simulations (Case A and Case B) are conducted. In Case A, the fluid is not allowed to flow in the fractures. On the other hand, the fluid is allowed to flow into the fractures in Case B. As the homogeneity index is very high ($m = 1000$) for these two simulations, two straight fractures open at both ends of the vertical diametrical line where the tensile stress is the highest. In the first simulation, since the fluid is not allowed to flow into the fractures, the results indicate that the growth of the cracks is controlled by the stress concentration near the crack tips due to the pressure inside the hole (Fig. 9). These fractures initiate at a pressure of 21.1 MPa and grow to a length of 15 mm at 31.7 MPa. The plot of the variations of diametric (vertical and horizontal) lengths versus the fluid pressure, as shown in Fig. 10, show that crack growth in the situation of fractures without fluid flow increases gradually, and therefore one can describe the failure process as a stable one until the breakdown pressure, 44.6 MPa, is reached.

However, one can find readily from Fig. 10 that the failure mode becomes unstable when fluid is allowed to flow into the fractures. It is seen that the fractures developed rapidly as they initiated at the circumference of the hole. The initiation pressure is 21.1 MPa and, immediately, the fluid pressure reaches a breakdown pressure at 21.2 MPa, that is 50% lower than the breakdown pressure for the situation without fluid flowing into the fractures.

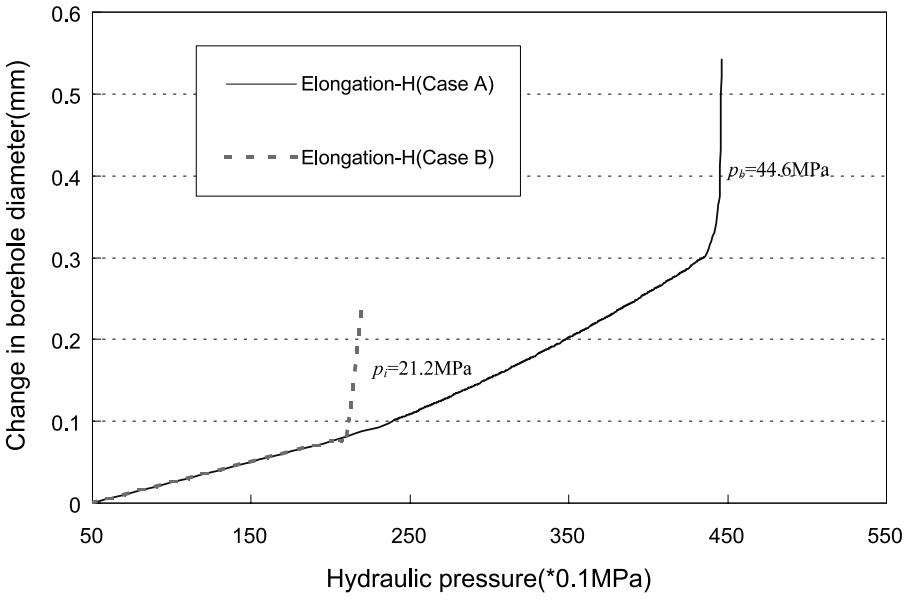

Fig. 10. Change in borehole diameter with hydraulic pressure – Case A and Case B

3. Numerical Results and Discussion on Influence of Heterogeneity on Hydraulic Fracturing

To study the influence of heterogeneity of mechanical properties on hydraulic fracturing in permeable rocks, analysis of fracture propagation in non-homogenous medium is required. It is well known that analytical solutions, which are based on general fracture mechanics, are not able to predict the growth of fractures in a heterogeneous material, especially when the fracture propagates under fluid pressure. It is necessary to resort to numerical means. Unlike the analytical solutions which are restricted to homogeneous materials, the present finite element model can easily simulate the heterogeneity (here randomly disordered material) by varying the homogeneity index m of Eq. (2). To study the influence of heterogeneity, a series of numerical simulations of hydraulic fracturing process using the theory and the numerical method described above is carried out.

The plane strain 2D model adopted in the study is shown in Fig. 11. The circular sample, which has a concentric opening representing the borehole, is discretized into $40401(201 \times 201)$ finite elements. The inner and outer diameters are 36 mm and 312 mm, respectively. Therefore, the ratio of the inner to outer diameters d/D is 0.115. Δd_{pa} and Δd_{pe}, as shown in Fig. 11, are defined as the diameter elongation of parallel and perpendicular directions with respect to crack orientation. L_U is defined as the unstable crack length, and *H-Line* is defined as the horizontal line through the holes. Hydraulic pressure is applied along the boundary of the interior hole. The rate of pressurization is kept constant throughout the numerical tests at 0.1 MPa/step.

The mechanical parameters, such as elastic modulus, the strength properties, and the permeability coefficient, etc., of the elements are all randomly assigned following a Weibull's distribution law to account for the inherited variability in rock property (Tang, 1997). Samples with five different homogeneity indices ($m = 1.5$, 2, 3, 6 and 20) are numerically tested (Fig. 12a–e). Other pertinent parameters of rock samples are shown in Table 2.

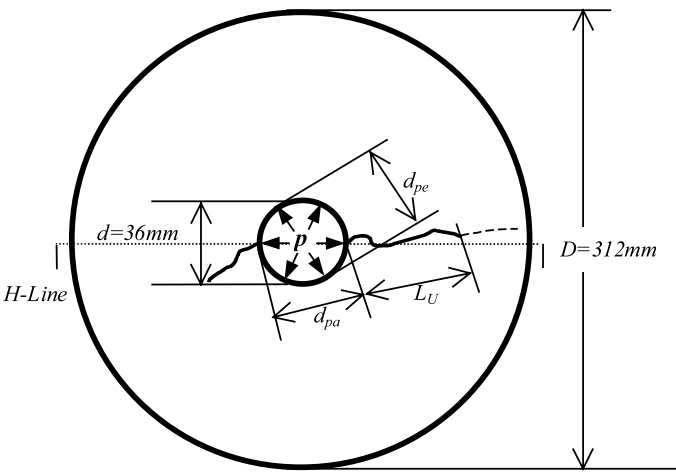

Fig. 11. Sample geometry for simulating hydraulic fracturing in rocks with different homogeneity indices

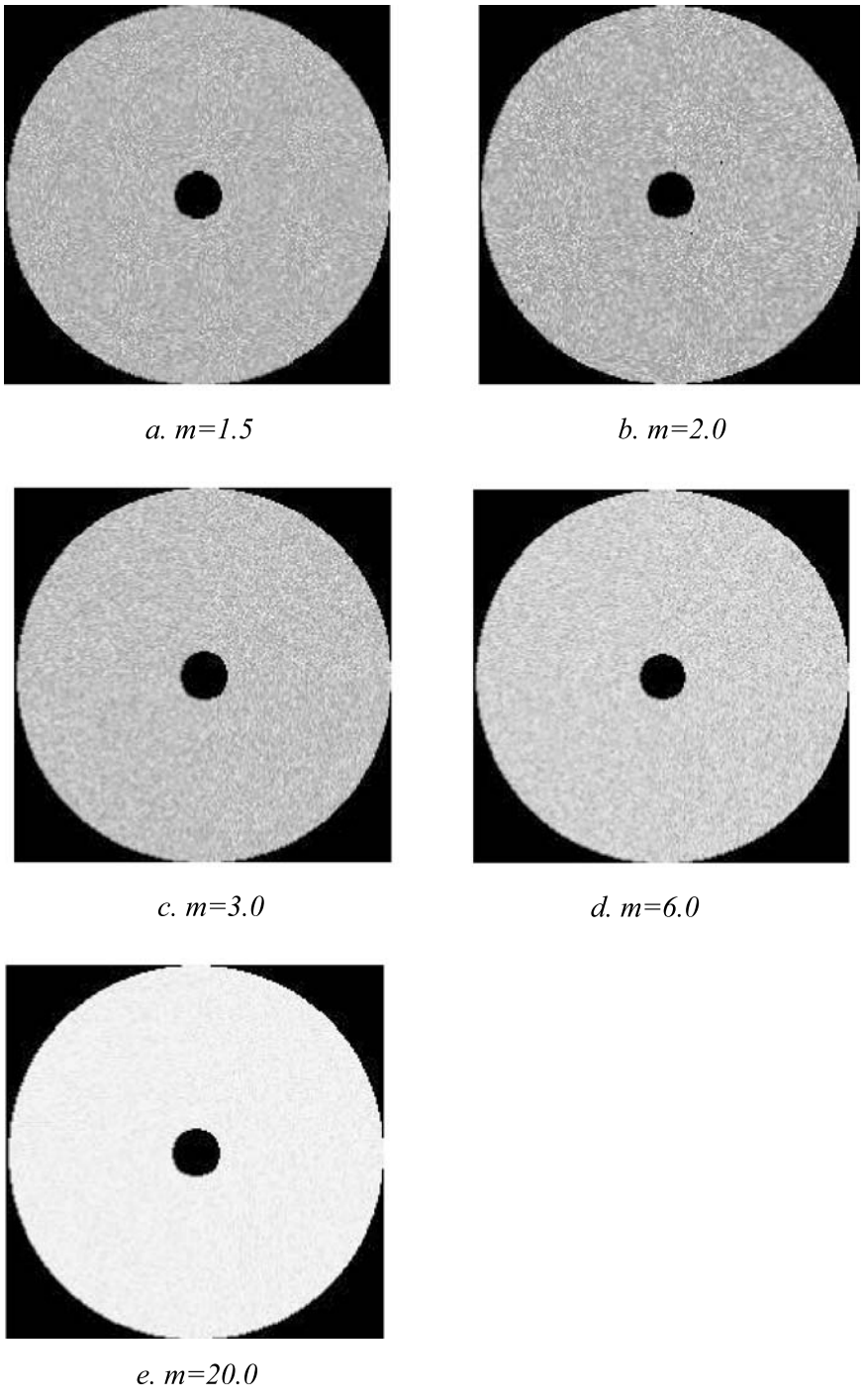

Fig. 12. Ring samples with different homogeneity indices (m = 1.5, 2, 3, 6 and 20)

Table 2. Input parameters of rock properties in hydraulic fracture simulations

m	1.5, 2, 3, 6, 20
E_0 (*mean elastic modulus*)	34 GPa
v	0.25
ϕ_0 (*mean friction angle*)	30°
f_{co} (*mean compressive strength*)	220 MPa
f_{to} (*mean tensile strength*)	22 MPa
λ	0.1
k_0 (*mean coefficient of permeability*)	0.01 m/sec
α (*unfractured*)	0.1
α (*fractured*)	1.0
β	0.05

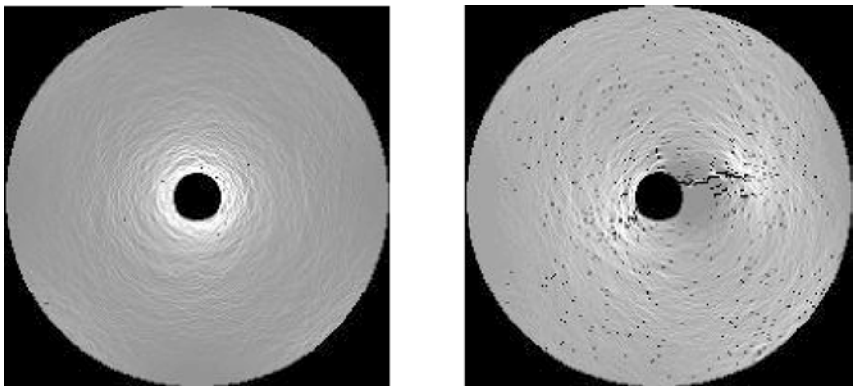

Fig. 13. Numerically obtained stress field evolution during hydraulic fracturing process in sample with homogeneity index $m = 1.5$

3.1 Stress Field

Only one case with homogeneity index $m = 1.5$ is discussed in the following. Fig. 13 shows the evolution of crack and stress field during the hydraulic fracturing process. As the hydraulic pressure in the borehole increases, the average maximum tensile stress increases along the boundary of the borehole wall. The bright areas at the immediate vicinity of the wall are the zones of highest tensile stresses. Generally speaking, there is no preferential location along the borehole wall for the fracture to initiate since the geometry of the sample is symmetrical. However, due to the heterogeneity of the sample, stress fluctuation occurs in the sample. Therefore, the location and orientation of the fracture initiation is unpredictable. As soon as the fracture initiates, the local heterogeneity will also affect the evolution of fracture patterns.

3.2 Hydraulic Fracture Path

As we know, the analysis of hydraulic fracture is plagued by the question of the validity of conventional fracture parameters such as critical stress intensity factor (Gorelic and Chudnovsky, 1996). These parameters are directly linked to the micro-mechanisms of hydraulic fracture. Fracture surface or hydraulic fracture propagation path is one of the sources of information regarding these micro-mechanisms (Horii and Okui, 1993).

Figure 14 displays the view of random pattern of a hydraulic fracture formed in the numerical modeling of hydraulic fracture in a sample with homogeneity index $m = 1.5$. The pattern closely resembles the experimentally observed hydraulic fracture path obtained in hydraulic fracture tests (Gorelic and Chudnovsky, 1996). The numerically obtained random nature of hydraulic fracture path during hydraulic fracturing and its dependence on inhomogeneities is illustrated in Fig. 15 for samples with $m = 1.5$ (relatively heterogeneous) and $m = 20$ (relatively homogeneous). It shows that the roughness of hydraulic fracture path is related to the homogeneity index of the rock. From the figures, one can conclude that the propagation of hydraulic fractures is controlled by the pre-existing field of defects. The hydraulic fracture deterministically selects a path of least resistance through the material with statistical features, and the random location of the individual inhomogeneities results in an irregular hydraulic fracture trajectory.

3.3 Comparison Analysis of Different Homogeneity Indices

Several snapshots of the fracture patterns and the associated stress fields taken from the loading steps for sample with homogeneity indices $m = 1.5$, 2, 3, 6 and 20 are presented in Fig. 16. From this figure, the following conclusions can be drawn:

1. as the homogeneity index m of material properties increases, the hydraulic fracture path becomes smooth, and
2. the strength increases while the stage of stable propagation becomes short-lived.

The study on the role of hydraulic fracturing shows that the strength of material is mostly dependent on mesoscopic homogeneity.

3.4 Elongation of Borehole Diameter and AE Behavior

Information of borehole diameter elongation during loading can improve the interpretation of hydraulic fracturing (Charlez, 1991). This problem consists of calculating the diameter elongation at the borehole wall for a given fracture length and a given internal pressure. In linear elasticity, this problem results in a very complicated analytical solution. In addition, analytical solutions cannot, to the best knowledge of the authors, provide the locations and energy levels of the acoustic emission activities during the development of cracks. Such information, diameter elongation and AE activities, can be easily obtained from the F-RFPA^{2D} simulation.

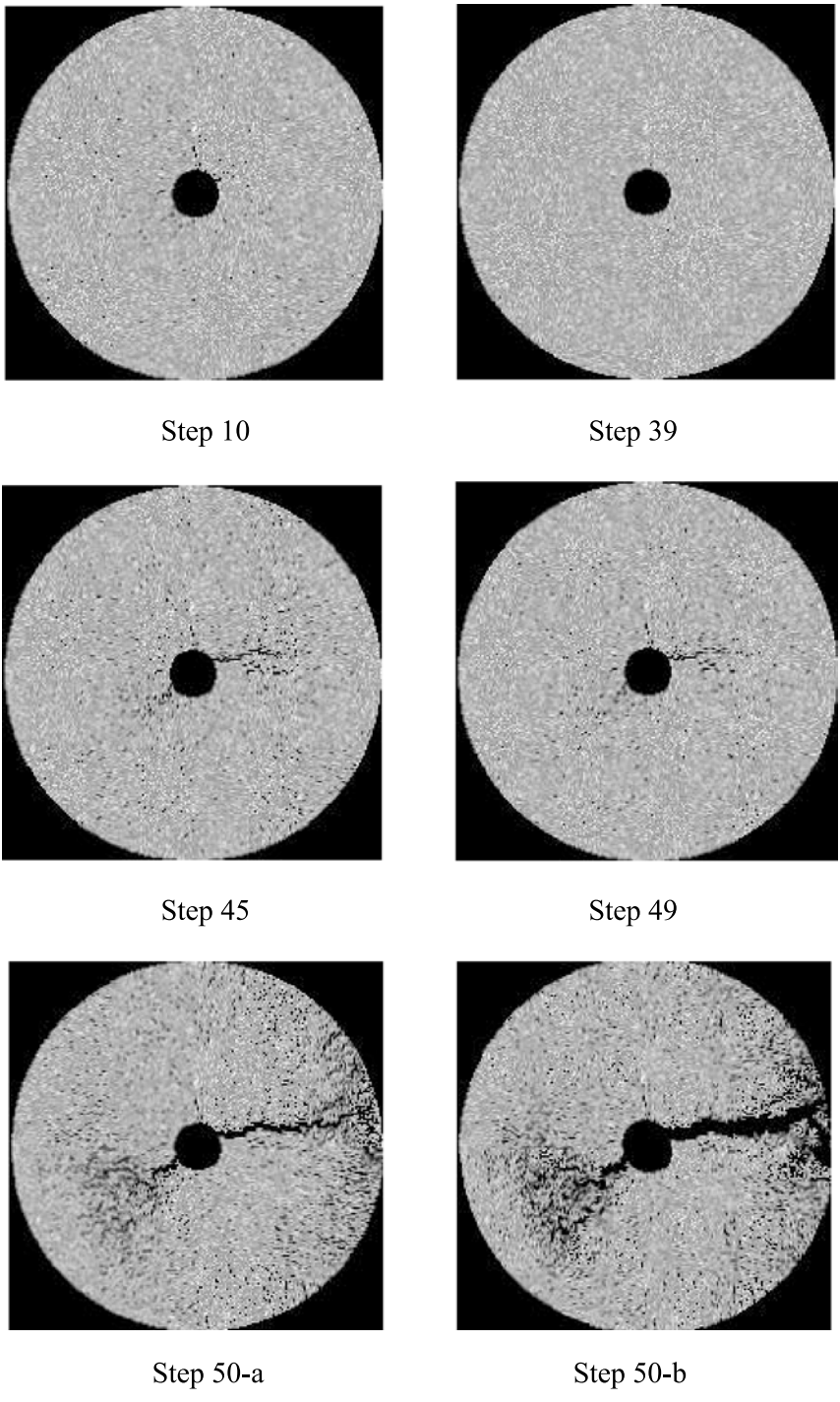

Fig. 14. Numerically obtained failure mode in sample with homogeneity index $m = 1.5$

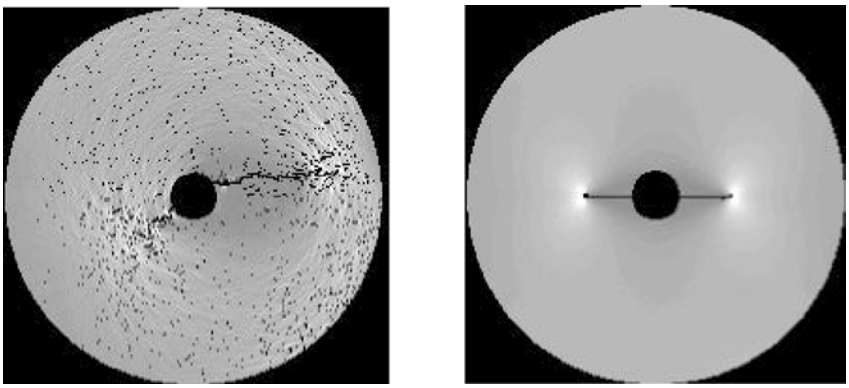

a. m=1.5 b. m=20

Fig. 15. Influence of heterogeneity on fracture path

Figure 17 shows the results of the borehole diameter elongation (Δd_{pe} and Δd_{pa}), and the AE rate for all the samples with different homogeneity indices. Before fracture initiation, the diameter elongation at the borehole wall is uniform and the slope of the diameter – pressure curve provides direct measurement of the hydraulic fracture behaviour. Comparing with the diameter elongation before fracture initiation, fracture initiation and propagation generate a strong anisotropy of diameter elongation along different directions. As shown in Fig. 17, as soon as the fracture initiates, the diameter elongation along the wall becomes anisotropic, and the diameter component being maximum perpendicular to the fracture and minimum in its own direction. This anisotropy amplifies as the fracture propagates.

Take the sample with homogeneity index $m = 1.5$ as an example; typically two stages of the hydraulic fracturing process, based on the borehole deformation behavior, are noted. They are:

(*1*) *Elastic deformation leading to fracture initiation.* In this stage, stresses accumulate (step = 1–34), as the internal pressure increases. The diameter of the borehole also increases proportionally with the borehole pressure until point *i* (step = 35). At this point, the diameter expansion (Δd_{pe}) at perpendicular direction abruptly increases at an accelerating rate (Fig. 17). The fracture initiation under pressure, P_i, occurs quite early before the peak (or breakdown) pressure, P_b, is reached. Acoustic emission is also activated immediately following point *i*. Figure 17 shows that the fracture initiation pressure is about 70% lower than the corresponding breakdown pressure.
(*2*) *Fracture growth leading to breakdown.* In the second stage, cracks propagate stably (*step* = 35–49, is defined as the state of cracks propagated under continually increasing hydraulic pressure). Beyond point *i*, due to the further increase in the borehole pressure, the diameter of the borehole continues to increase drastically, and hence to widen the fracture and drive the fracture to propagate. The constant rate of diameter increase suggests a stable fracture propagation. At point *b* (*step* = 50), the borehole diameter elongation and the AE rate increase drastically (Fig. 17), as the

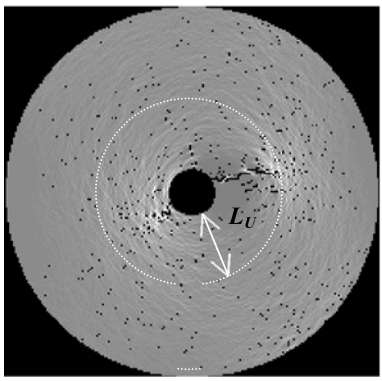

a. m=1.5, P_u=5.0MPa, L_u=69.9mm

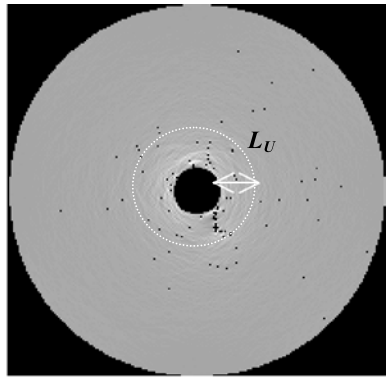

b. m=2.0, P_u=6.6MPa, L_u=24.8mm

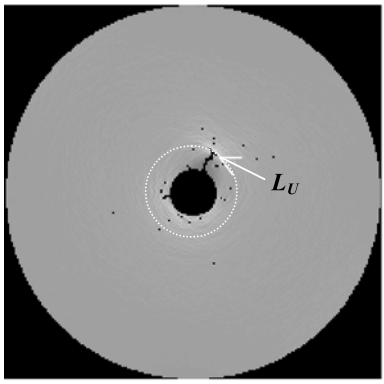

c. m=3.0, P_u=8.8MPa, L_U=15.5mm

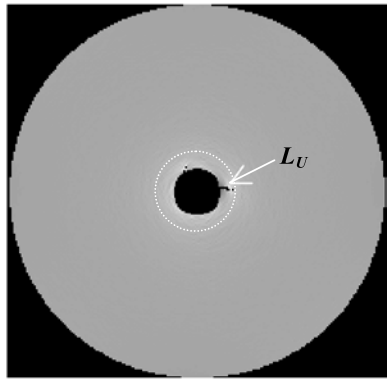

d. m=6.0, P_u=11.0MPa, L_U=9.3mm

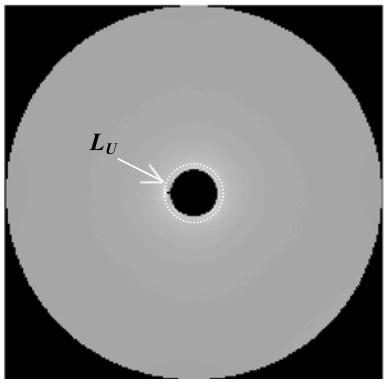

e. m=20, P_u=14.0MPa, L_U=3.1mm

Fig. 16. Stress field and fracture mode of ring samples during the hydraulic fracturing process with different homogeneity indices (m = 1.5, 2, 3 ,6 and 20)

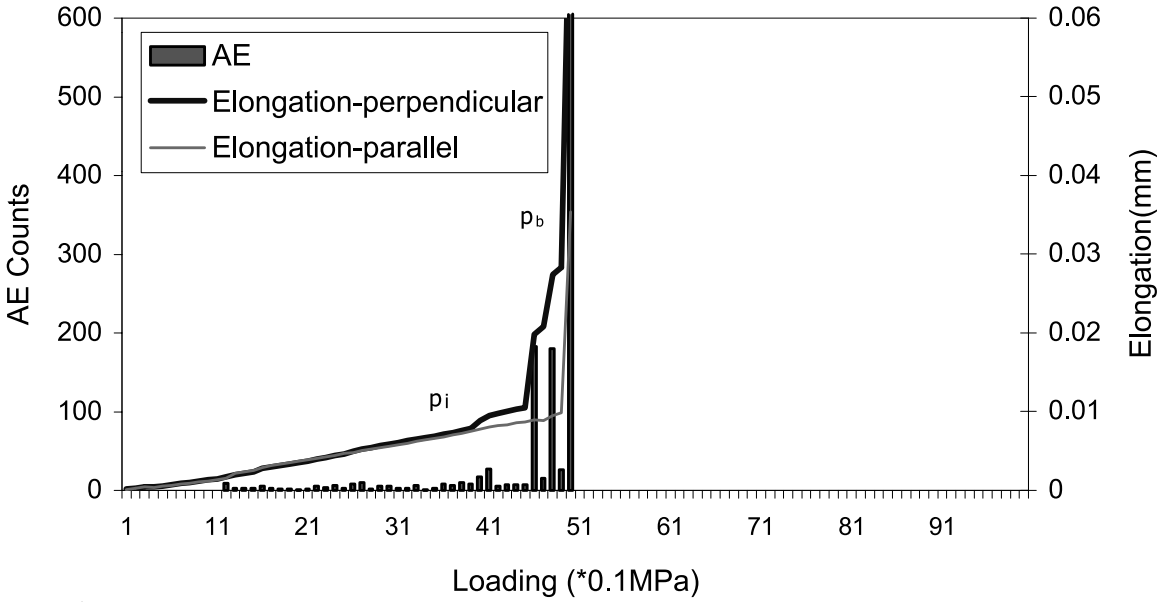

a.m=1.5

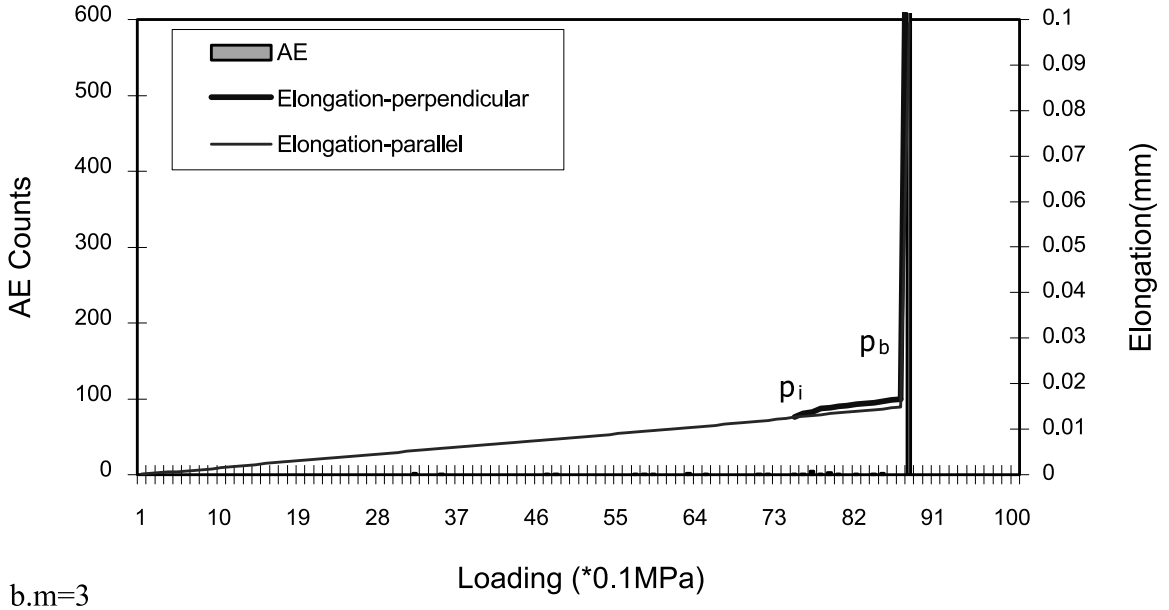

b.m=3

Fig. 17. Influence of heterogeneity on AE counts and borehole diameter variation ($m = 1.5$ and 3)

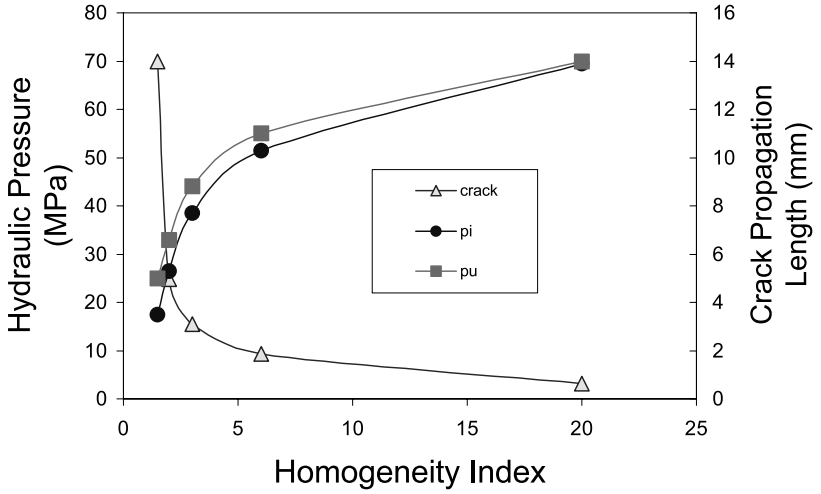

Fig. 18. Influence of heterogeneity on crack initiation pressure P_i, breakdown pressure P_U and unstable crack length L_U of samples with $m = 1.5$, 2, 3, 6, 20

pressure reaches its peak level (breakdown pressure P_b), which indicates the unstable propagation without increasing pressure. When the pressure is close to the breakdown pressure, the length of crack (L_U) is defined as the unstable crack length.

For a sample with homogeneity index $m = 1.5$, the development of fracture is shown in Fig. 14. From Fig. 16, one can obtain that $P_i = 3.5$ MPa, $P_b = 5.0$ MPa, $L_U = 69.85$ mm. These parameters for other samples (homogeneity index $m = 2$, 3, 6 and 20) can be obtained from Fig. 18. The results regarding diameter elongation agree well with the results obtained by Charlez (1991) using Displacement Discontinuity Method. Since we use the loading condition of constant rate of pressure, the loading process becomes unstable as soon as the breakdown pressure is reached. Therefore, no fracture closing stage as observed in the experiments of Zhao et al. (1996) is observed in our simulation.

3.5 Initiation, Unstable Propagation and Breakdown Pressure

The conventional interpretation of the hydraulic fracturing process has been that the breakdown pressure, P_b, reached during pressurization of the borehole test interval signifies the instance of hydraulic fracture initiation. Recently, Detournay and Carbonell (1994) have challenged the assumption that hydraulic fractures necessarily initiate at P_b. They distinguished three different critical pressures: (**1**) fracture initiation pressure, P_i; (**2**) unstable propagation pressure, P_u; and (**3**) breakdown (or peak) pressure, P_b. The so-called unstable propagation fracture is defined as the state of continued crack propagation without increasing the pressure. According to their investigation, they speculate that the condition of unstable fracture propagation is in fact equal to the breakdown pressure, i.e., $P_u = P_b$. They also concluded that at slow

pressurization rates and uniform far-field stress condition fracture initiation always results in unstable propagation. In the condition that the two horizontal far-field stresses are unequal, they showed that the fracture propagation after initiation could be stable or unstable, which implies that the fracture initiation pressure in this case may be smaller than the breakdown pressure. Zhao et al. (1996) also obtained similar results.

Figure 18 shows the fracture initiation pressure and breakdown pressure for sample with homogeneity index $m = 1.5$, 2, 3, 6 and 20. The simulations reveal that both pressures are influenced considerably by rock heterogeneity. When the sample is homogeneous, the fracture initiation pressure is very close to the value of the breakdown pressure, unstable crack length is shorter. On the other hand, significant difference between the two pressure values is observed and the unstable crack length is longer for the heterogeneous samples. The numerical simulations also show that both fracture initiation and breakdown pressure values are much higher for the homogeneous sample than those for the heterogeneous sample.

4. Conclusions

The numerical simulations using flow-coupled Rock Failure Process Analysis code, F-RFPA^{2D}, clearly indicate that both the rock heterogeneity and the permeability affect fracture initiation and propagation significantly. Our findings are:

(1) Heterogeneity of rock has a significant influence on the initiation and breakdown pressure. For heterogeneous rock samples, hydraulic fracture initiation occurs considerably earlier before the breakdown pressure is reached. While for homogeneous samples, the fracture initiation pressure and breakdown pressure are indistinguishable. Both fracture initiation and breakdown pressure values are much higher for the homogeneous sample than those for the heterogeneous sample.
(2) The hydraulic fracture path is also considerably influenced by the heterogeneity of the rock samples. The random location of the individual inhomogeneities results in an irregular hydraulic fracture trajectory.
(3) The elongation in borehole diameter is a reasonable sign to indicate the location of fracture initiation. For the borehole diameter at right angles to the direction of hydraulic initiation, the initial linear elongation – pressure signifies elastic behavior. A sudden acceleration in the rate of diameter elongation represents the fracture initiation, and the maximum diameter corresponds to breakdown.
(4) The hydraulic pressure in the crack plays an important role to propagate the fracture. It can also be inferred, based on the results of other authors, that the pressurizing fluid flowing into the cracks is the main factor.
(5) The F-RFPA^{2D} clearly simulates the hydraulic fracturing in heterogeneous rocks in a more realistic way than other numerical models. The capability of F-RFPA^{2D} in identifying hydraulic fracturing modes is obvious. Therefore, it is concluded that the flow-coupled F-RFPA^{2D} is a useful tool in understanding the physics of hydraulic fracturing, especially in heterogeneous and permeable materials.

Acknowledgement

The study presented in this paper is supported by the Research Grants Council of HKSARG (HKU7029/02E) and the China NSFC (50204003, 50134040 and 50174013). It is also partially supported by the Department of Civil Engineering, the University of Hong Kong.

References

Aamodt, R. L., Potter, R. M. (1978): Anomalous fracture extension pressures in granite rocks, 19th U.S. Rock Mechanics Symposium, Stateline, Nevada, 10–13.

Advani, S. H., Lee, T. S., Lee, J. K. (1990): Three-dimensional modeling of hydraulic fracture in layered media. ASME J. Energy Resour. Technol. 112, 1–9.

Biot, M. A. (1941): General theory of three-dimensional consolidation. J. Appl. Phys. 155–164.

Brown, S., Caprihan, A., Hardy, R. (1998): Experimental observation of fluid flow channels in a single fracture. J. Geophys. Res. 103, 5125–5132.

Charlez, P. A. (1991): Rock mechanics II: Petroleum applications. Technical Publisher, Paris.

Degue, K. M., Ladanyi, B. (2000): Effect of fluid penetration and pressurizing rate on hydraulic fracturing. In: Girad, J., Liebman, M., Breed, C., Doe, T. (eds), Pacific rocks 2000, Balkema, Rotterdam, 181–188.

Detournay, E., Carbonell, R. (1994): Fracture mechanics analysis of breakdown process in minifrac or leak-off tests. In: Proc., Eurock'94, Balkema, Rotterdam, 399–407.

Haimson, B. (1968): Hydraulic fracturing in porous and non porous rock and its potential for determining in-situ stress at depth. Ph.D. Thesis, University of Minnesota, Misseapolis, MN.

Haimson, B., Fairhurst, C. (1969): Hydraulic fracturing in porous-permeable materials. J. Petrol. Technol. 21, 811–817.

Gorelic, M., Chudnovsky, A. (1996): Application of statistical fracture mechanics in hydraulic fracture. In: Aubertin, M., Hassani, F., Mitra, H. (eds), Rock mechanics: Tools and techniques, Balkema, Rotterdam, 1261–1268.

Horii, H., Okui, Y. (1993): Thermo mechanics and micro mechanics-based continuum theory for localization phenomena. In: Baker, G., Karihaloo, B. L. (eds), Proc., IUMAM Symposium on Fracture of Brittle, disordered materials, 391–405.

Hubbert, M. K., Willis, D. G. (1957): Mechanics of hydraulic fracturing. Trans. AIME. 210, 153–166.

Kim, K., Yao, C. Y. (1994): The influence of constitutive behaviour on the fracture process zone and stress field evolution during hydraulic fracturing. In: Nelson, P. P., Laubach, S. E. (eds), Rock mechanics: Models and measurements challenges from industry, Balkema, Rotterdam, 193–200.

Lockner, D., Byerlee, J. D. (1977): Hydrofracture in Weber sandstone at high confining pressure and differential stress. J. Geophys. Res. 82(14), 2018–2026.

Louis, C. (1974): Rock hydraulics, In: Muller, L. (ed), Rock mechanics. Springer-Verlag, Wien-New York, 300–387.

Morale, R. H., Abou-Sayed, A. S. (1989): Microcomputer analysis of hydraulic fracture behaviour with a pseudo-three-dimensional simulator. SPE Production Engineering 4, 69–74.

Rummel, F. (1987): Fracture mechanics approach to hydraulic fracturing stress measurements. In: Atkinson, B. (ed.), Fracture mechanics of rock. Academic Press, New York, 217–239.

Rummel, F., Hansen, J. (1989): Interpretation of hydrofrac pressure recordings using a simple fracture mechanics simulation model, Int. J. Rock Mech. Min. Sci. Geomech Abstr 26: 483–488.

Rummel, F., Klee, G., Weber, U. (1995): Hydraulic vs pneumatic fracturing for *in situ* stress determination in rock salt, Int. J. Rock Mech. Min. Sci. Geomech Abstr 32: 337–342.

Tang, C. A. (1997): Numerical simulation on progressive failure leading to collapse and associated seismicity. Int. J. Rock Mech. Min. Sci. 34: 249–262.

Tang, C. A., Tham, L. G., Lee, P. K. K., Yang, T. H. (2002): Coupled analysis of flow, stress and damage (FSD) in rock failure. Int. J. Rock Mech. Min. Sci. 39: 477–489.

Wang, R. Q., Kemeny, J. M. (1994): A study of the coupling between mechanical loading and flow properties in tuffaceous rock. In: Nelson, P. P., Laubach, S. E. (eds), Rock mechanics: Models and measurements challenges from industry, Balkema, Rotterdam, 749–756.

Yale, D. P., Lyons, S. L., Qin, G. (2000): Coupled geomechanics-fluid flow modeling in petroleum reservoirs: coupled versus uncoupled response. In: Girard, J., Liebman, M., Breed, C., Doe, T. (eds), Pacific rocks 2000, Balkema, Rotterdam, 137–144.

Yang, T. H., Tang, C. A., Zhu, W. C., Feng, Q. Y. (2001): Coupling analysis of seepage and stress in rock failure process. Chin. J. Geotechni. Engng. 23(4), 489–493.

Zhang, J. C., Bai, M., Roegiers, J. C., Wang, J. X., Liu, T. Q. (2000): Experimental determination of stress-permeability relationship. In: Girard, J., Liebman, M., Breed, C., Doe, T. (eds), Pacific rocks 2000, Balkema, Rotterdam, 817–822.

Zhu, W. L., Wong, T. F. (1999): Network modeling of the evolution of permeability and dilatancy in compact rock. J. Geophys. Res. 104(B2), 2963–2971.

Zoback, M. D., Pollard, D. D. (1978): Hydraulic fracture propagation and the interpretation of the pressure-time records for In-situ stress determination. 19th U.S. Rock Mechanics Symposium, Stateline, Nevada. 14–22.

Zhang, B. C., Wu, H. M., Liu, C. Y. (1991): The effect of stress on pore pressure in rocks and the mechanism of water table anomaly before earthquakes. Acta Seismologica Sinica (Chinese) 13(1): 88–95.

Zhao, Z., Kim, H., Haimson, B. (1996): Hydraulic fracturing initiation in granite. In: Aubertin, M., Hassani, F., Mitra, H. (eds), Rock mechanics: Tools and techniques, Balkema, Rotterdam, 1279–1284.

Authors' address: Dr. L. G. Tham, Department of Civil Engineering, The University of Hong Kong, Hong Kong, China. E-mail: hrectlg@hkucc.hku.hk